Research Article

Cristian F. Ramirez-Gutierrez*, Jorge D. Castaño-Yepes, and Mario E. Rodriguez-Garcia

Optical interferometry and photoacoustics as in-situ techniques to characterize the porous silicon formation: a review

https://doi.org/10.1515/oms-2018-0003
Received Mar 12, 2018; revised Apr 09, 2018; accepted May 11, 2018

Abstract: Porous Silicon (PSi) is a groundbreaking material because its physicochemical properties can be customized through its porosity. This means that monitoring and control of the growing parameters allows the fabrication of PSi-based systems with controlled properties. Interferometry and photoacoustics are non -invasive, non -contact, real-time (in-situ) techniques used to characterize the phenomena that takes place during the formation of PSi. This work presents the mathematical and experimental aspects related to the implementation of the techniques mentioned above, which are meant to characterize the PSi growth in fluoride-based electrolyte media. These methods can determine macroscopic parameters of PSi such as thickness, porosity profile trough effective medium approximation (EMA), refractive index, etching rate, and RMS roughness under 100 nm. The monitoring ability of these techniques is strongly dependent on the wavelength of radiation used. However, it is possible to monitor thickness from $\lambda_0/4$ to $\sim 1/\alpha_0$, where α_0 is the optical absorption coefficient at λ_0. Also, these techniques can be implemented as feedback control on the etching processes for fabrication of PSi.

Keywords: porosity, effective medium , optical properties, thickness, etching rate

***Corresponding Author: Cristian F. Ramirez-Gutierrez:** Posgrado en Ciencia e Ingeniería de Materiales, Universidad Nacional Autóma de México, Campus Juriquilla, CP 76230, Querétaro, Qro., Mexico; Email:cframirezg@comunidad.unam.mx
Jorge D. Castaño-Yepes: Instituto de Ciencias Nucleares, Universidad Nacional Autónoma de México, CP 04510, Ciudad de México, México; Email: jorge.castano@correo.nucleares.unam.mx
Mario E. Rodriguez-Garcia: Departamento de Nanotecnología, Centro de Física Aplicada y Tecnología Avanzada, Universidad Nacional Autóma de México, Campus Juriquilla, CP 76230, Querétaro, Qro., Mexico; Email: marioga@fata.unam.mx

1 Introduction

In the last decades, the physical modification of the well-known materials, like silicon and carbon, has become a tendency since the demand for customized systems is a constant requirement, particularly for the optoelectronic industry. The primary objective of this kind of processes is to change the physicochemical properties of materials or give them new ones. These modifications are related to structure, morphology, and dimensionality [1]. Another way to modify the features of the materials is through the chemical route, which mainly consists in the formation of new compounds and functionalization [2, 3]. Porous silicon (PSi) is an excellent example of the new functionality of crystalline silicon (c-Si). PSi consists of a porosified matrix of c-Si, which confers it with different properties compared with the bulk material, making it an interesting system for various fields such as electronics, optoelectronics, photonics, bioengineering, and chemical sensing.

PSi material can also be applied to the manufacturing of Lithium-ion batteries (LIBs). In this way, Si may present a high energy density, but its structure goes through a volume expansion upon the lithidation, producing a cracking in the electrode and resulting in an energy capacity loss. An alternative to solve this problem is to use a porosified matrix of Si (PSi) as anodes that can hold the strain, [4–7] which requires high accuracy and reproducibility in size and morphology of the PSi anodes. The main issues of PSi are the porosity and surface chemistry, because the mechanical, electrical, optical, and thermal properties depend effectively on these parameters. At the same time, the porosity is determined by the parameters involved in the fabrication process. Hence, it is the primary property to be controlled.

The PSi is usually obtained by anodization or electrochemical etching in presence of aqueous fluoride media. However, other routes have been developed, like vapor etching, photoetching, alkali-based etches, among others [8]. Canham presented different fabrication techniques in Ref. [8], and the formation mechanisms have been de-

scribed by Smith and Collins [9]. Although the models of formation had been proposed, the properties of the PSi system are strongly dependent on intrinsic parameters (*e.g.*, wafer crystalline orientation, type and doping concentration, defects) and extrinsic parameters (*e.g.*, temperature, electrolyte composition, anodization current, operator skills), and the characterization of PSi is usually carried out *ex situ*. These critical aspects require methods for monitoring several parameters during the etching of PSi.

The main techniques reported to study the *in situ* formation of PSi by electrochemical etching in hydrofluoric acid(HF) media are: *in situ* Fourier transform infrared spectrometry (FTIR) [10, 11], optical interferometry [12–17] optical scattering [19, 20], and photoacoustics [21–25].

The previous reports about the *in situ* characterization of the PSi etching focused on studying the chemical kinetics of the etching reaction and the optical properties (film thickness, refractive index, porosity, roughness). Rao et al. [10] used FTIR spectroscopy to study the chemical species that appear during the etching. They found that the Si-H species are always present on the Si surface, even when the PSi is drying. This technique provides direct evidence of the incorporation of H into Si lattice [26]. The SiH_x becomes important because it partially explains the photoluminescence of PSi [27–30].

The self-organization in PSi formation explains experimental features in the morphological properties of PSi such as a constant porosity profile, and the surface roughness [31]. Consequently, the optical properties of PSi result an effective combination of the optical properties of Si bulk and the material, which is embedded in the porous matrix. This means, that during the PSi formation, it is possible to follow the changes in the thickness, roughness, and porosity by using light interferometry because the optical path changes continuously and multiple interfaces where the light can be reflected appear. This methodology and the mathematical model were reported in [12–18].

Another technique is photoacoustics, which consists in sound generation by the modulated light absorption [32]. Photoacoustic techniques are nondestructive and are used to study thermal and optical properties of several materials, including porous media [33–35]. It is crucial to highlight that there are two methodologies to study materials using photoacoustic. In the first one, the measurement is carried out when the sample does not present physical or chemical changes, even with the interaction with radiation. These measures are usually performed as a function of the frequency of the modulated light, and used to determine thermal properties. The second one can be used to study kinetic processes; it means that the sample changes during the measure. It is useful to follow changes in optical and thermal properties in real time, the formation of multilayers, wetting process [21] , emptying and filling of porous media, and chemical reactions. Indeed, it is possible to perform an *in situ* monitoring of the PSi formation by using photoacoustic in HF aqueous media [21–25].

This work shows the theoretical models and experimental issues related to the *in situ* characterization techniques of PSi formation. The first topic is related to the interferometry techniques, using front and back illumination with sub-bandgap radiation. These methodologies are useful to estimate the etching rate, roughness, and porosity of PSi. The second method is photoacoustics. In this technique a super-bandgap radiation is required in order to produce the thermal wave formed by the diffusion of electrons and phonons, which generates a sound signal after the de-excitation process. This method is used to determine the refractive index, etching rate, porosity, and to design multilayers systems of PSi.

2 Porous silicon formation

Electrochemical etching is the most common route to obtain PSi. Admittedly, the usual geometrical arrangement of the electrochemical cell is formed by two-electrodes where the working electrode is c-Si (anode), and the counter-electrode is platinum (cathode). Figure 1 shows a schematic representation of the generic etch cell.

The physicochemical explanation of how the pores are formed is still an open problem because multiple chemical reactions take place during the etching. Despite this, the chemical reaction proposed by Lehmann and Gösele [36] (Eq. 1) is useful to understand that the reaction needs positive charges (holes) and releases hydrogen.

The current-voltage curve in HF media exhibits three main regions [37]. It is necessary to overcome the V_{OCP} (open circuit potential) to start the etching. At increasing positive potential, the first region shows an exponential behavior and the porous formation is regular. Next, the second region is a transition stage characterized by an irregular formation of porous. When a maximum current density (critical current) is reached, the electropolishing occurs; this is the third region.

$$Si + 6F^- + 2H^+ + 2h^+ \rightarrow SiF_6^{2-} + H_2 \quad (1)$$

At this point, it is essential to take into account some issues related to experiment performance that influence the formation of PSi. For a homogeneous etching, it is crucial to clean the sample following the RCA [38, 39] standard method or sonication [40], and to guarantee ohmic con-

tacts even for highly doped samples. Even so, it is possible to find resistivity variations because the dopant distribution in the Si wafer is nonhomogeneous.

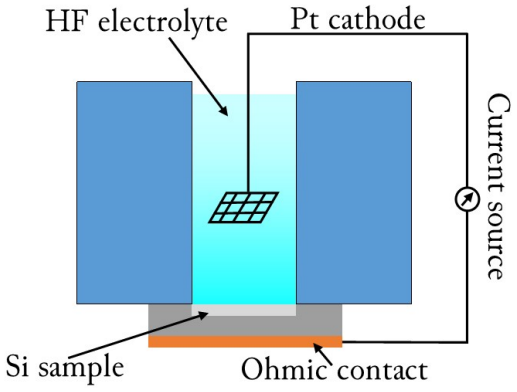

Figure 1: Schematic of the electrochemical cell. The Si sample seals the electrolyte reservoir. Also, the cell has to be HF-resistant

The composition of the electrolyte is also important. Commonly, the electrolyte base is an aqueous HF (37-40%) added with a surfactant (*e.g.*, ethanol or glycerol) to decrease the surface tension, which results in a better wettability [21]. The temperature of the electrolyte reservoir and the HF/surfactant ratio are the parameters that strongly influence the roughness of the PSi films [41].

Finally, the geometric cell configuration (reservoir and Pt electrode) influences the distribution of the current density. During the etching, a controlled current source injects a specific current profile. However, a constant current is more desirable provide a greater control of the thickness and porosity of the films.

3 Interferometry techniques

The base of these methodologies is interferometry. This is about the determination of the changes in reflected (reflectance, 'R') or transmitted (transmittance,'T') light intensity by the thin film structure. Also, it is possible to measure the electric field properties such polarization of the light (spectroscopic ellipsometry (SE)) [42]. In the case of PSi growth is possible to integrate an optical system to the electrochemical cell. Thus, during the PSi formation, new films and interfaces appear producing changes in the optical path [13]. The behavior of R, T, and polarization of the light contain information about the etch rate, optical constants, interface roughness, and porosity [16, 42].

Figure 2 shows a diagram of the situation. During the PSi formation, new interfaces appear, where the light can be reflected, and the optical path changes continuously making alternations of constructive and destructive interference. Two optical configurations can be used for etching monitoring. The first one deals with front illumination [14, 15]. The other one is related to the back illumination of the sample [13, 16]. In both cases, sub-bandgap radiation is recommended because Si has low absorbance for energies lower than Si band gap (1.12 eV). However, it is recommended a careful selection of the laser wavelength because the absorption coefficient is dependent on doped concentration due to free carries [47]. The absorption limits the thickness that the technique can monitor.

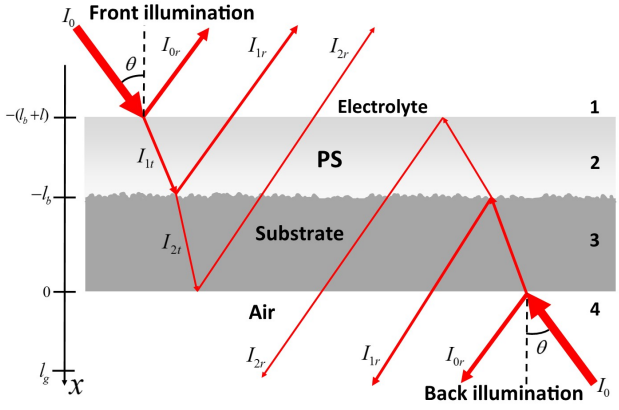

Figure 2: Ray trajectories through the sample during the etching. Two configurations are possible; by front or back incidence. The rough surface of PSi/Si interface produces light scattering

The reflection coefficients r_s (for s polarization) and r_p (for p polarization) are dependent of thickness, refractive index and interface roughness of each layer. In the case of reflectometry for an arbitrary angle of incidence the effective reflectance is expressed as

$$R_{eff} = \frac{1}{2}\left(|r_s|^2 + |r_p|^2\right), \tag{2}$$

while for ellipsometry the aim is to measure the changes of the reflectance ratio as

$$\rho = \frac{r_p}{r_s} = \tan(\Psi)e^{i\Delta}, \tag{3}$$

where Ψ is the ratio of reflected amplitudes and Δ is the phase difference produced upon reflection [42]. Moreover, (Ψ, Δ) are wavelength dependent. There are few works about in-situ SE to study the PSi formation [42–46].

3.1 Interferometry theory

Assuming monochromatic plane waves, the interference between the reflected and the incident waves is given by phase difference ($\delta(t)$). Using the diagram showed in figure 2, in the case of front illumination, the phase difference can be expressed as [14, 15]

$$\delta_F(t) = \frac{2}{\lambda_0}\sqrt{n_2(x)^2 - n_1^2\sin^2(\theta)}l(t) + \Delta\phi, \tag{4}$$

or in the case of back illumination

$$\delta_B(t) = \frac{2}{\lambda_0}\sqrt{n_3^2 - n_4^2\sin^2(\theta)}l_b(t) + \Delta\phi, \tag{5}$$

where n_i is the refractive index of the medium, θ is the incidence angle, and $\Delta\phi$ is the phase change of the reflected beam that is assumed as a constant.

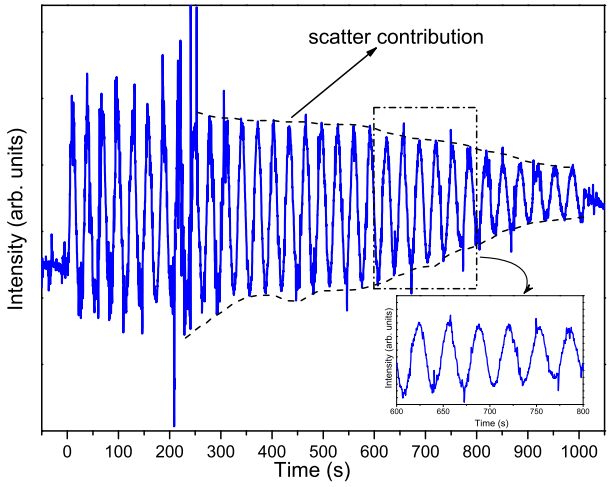

Figure 3: The intensity of the radiation during the etching of a sample with 3:7 ethanol/HF volume ratio. It was used a diode laser with a line 1550 nm and 10mA/cm^2.

The changes in the reflected intensity is proportional to $v(t)$; that it is the interference frequency.

$$v(t) = \frac{\partial\delta(t)}{\partial t} \tag{6}$$

In the case of the equations 4 and 5, the thickness of the PSi changes as a function of time as well as thickness of the Si substrate. These equations contain information about the refractive index, thickness, and etching rate of PSi. Also, it is possible to estimate the roughness of the film.

Figure 3 shows the intensity of the reflected radiation during the etching. In this case, the sample is illuminated from the front. Even though the absorption coefficient for Si is low at 1550 nm, the curve exhibits damping as a function of time. This effect is a scattering process due to the formation of rough interfaces.

Also, the inset in the figure 3 shows little jumps because there are hydrogen bubbles that could appear through the path of the light. It is possible to determine a value of the roughness that is described in the section 3.4.

Indeed, the subsequent analysis of these equations and the geometrical configuration can provide control of the etching process. The next study explores the methodologies reported for back and front illumination.

3.2 Double beam front illumination

The refractive index of the PSi is a function of depth. As it is defined in the equation 6, the oscillations in the reflected light change as a function of the thickness of the PSi film. Moreover, this equation has two unknown parameters; the refractive index profile and the velocity formation of PSi. If the sample is illuminated with two beams at different angles, it obtains two oscillation frequencies given by [15]:

$$v_i(t) = \frac{2}{\lambda_0}\sqrt{n_2^2(x) - n_1^2\sin^2\theta_i}\frac{dl(t)}{dt} \tag{7}$$

The equation 7 represents a system of equations with the following solution:

$$\begin{aligned} n_2(t) &= n_1\sqrt{\frac{v_1^2(t)\sin^2\theta_2 - v_2^2(t)\sin^2\theta_1}{v_1^2(t) - v_2^2(t)}} \\ \frac{dl(t)}{dt} &= \frac{\lambda_0}{2n_1}\sqrt{\frac{v_1^2(t) - v_2^2(t)}{\sin^2\theta_2 - \sin^2\theta_1}} \end{aligned} \tag{8}$$

The equation 8 describes a simple methodology to determine the refractive index and the etching rate during the PSi formation. Also, it is possible to determine the porosity profile by using an effective media rule [48] and the refractive index calculated by this method. To improve the accuracy of the refractive index and thickness estimation, is recommended a significant difference between the two incidence angles [49].

3.3 Back illumination

By using the equation 5, the etching rate is defines as it follows

$$r(t) = \left|\frac{d}{dt}l_b(t)\right| = \frac{\lambda_0}{2}\frac{1}{\sqrt{n_3^2 - n_4^2\sin^2\theta}}v(t). \tag{9}$$

However, equation 9 does not contain information of PSi layer. But, if the optical path of the beam that reflects in

the PSi/electrolyte interface is taken into account, a second phase difference can be defined as

$$\delta'_B(t) = \frac{2}{\lambda_0}\sqrt{n_3^2 - n_4^2\sin^2\theta}\, l_b(t) + \frac{2}{\lambda_0}\int_0^{l(t)}\sqrt{n_2^2(x) - n_4^2\sin^2\theta}\, dx, \tag{10}$$

and by using the expression 5, 9, and deriving the equation 10 to determine the interference frequency ν', the refractive index of the PSi is

$$n_2(l(t)) = \sqrt{\left(\sqrt{n_3^2 - n_4^2\sin^2\theta} - \frac{\lambda_0\nu'(t)}{2r(t)}\right)^2 + n_4^2\sin^2\theta}. \tag{11}$$

Equations 9 and 11 give the etching rate and the refractive index profile. The refractive profile can be used to determine the porosity by using an effective medium theory [48].

3.4 Roughness calculation by back illumination

In the case of the signal shown in the figure 3, the intensity falls off with time despite the fact that the absorption coefficient for Si in the IR range is very low. This effect is an indicator of the increase of the roughness that produces scattering during the PSi formation.

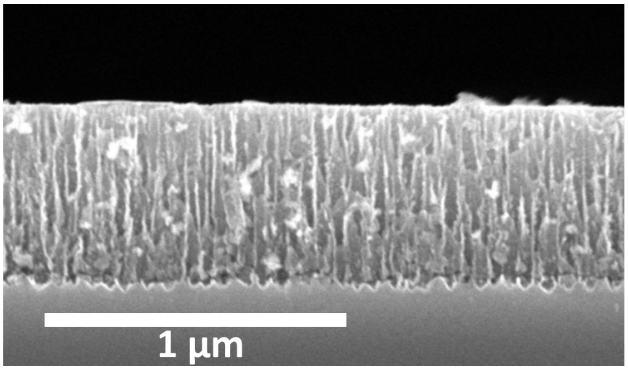

Figure 4: Cross section of a single layer of PSi. It is appreciated that the ends of the pores are not flat. This roughness causes scattering in the light

Figure 4 shows a cross-section of a PSi film. It is clear that the end of the pores does not have flat terminations. This rough interface and the porous branching, attenuate the amplitude of the reflected radiation. This effect allows to quantify the root mean square (RMS) roughness. In the case of the work reported by Kan et al. [17], they defined a parameter that described the scattering during the PSi formation as:

$$Roughness = \frac{A_{max} - A(t)}{A_{max}}. \tag{12}$$

The equation 12 is not a direct quantification of the roughness, but it provides a behavior of the light scattering during the PSi formation that is useful to determine the effect of the electrolyte composition. Nevertheless, to characterize the irregularities of the PSi/Si interface in the case of a single layer, it is possible to introduce the factor σ (RMS roughness), that in the case of $\sigma << \lambda_0$ and a Gaussian distribution, introduces a correction in the Fresnel reflection coefficient. The correction for back illumination can be written as follows

$$R_3 = R_0\exp\left[-\left(\frac{4\pi n_3\sigma_{2,3}}{\lambda_0\cos\theta}\right)^2\right], \tag{13}$$

where R_0 is the regular Fresnel coefficient (perfect flats surface), $\sigma_{2,3}$ is the RMS roughness between the material 2 and 3 (Si/PSi).This approximation is valid for roughness values $\sigma_{max} = \left(\sqrt{2}\lambda_0\right) / \left(8\pi n(\lambda_0)\right)$ [50, 51].

4 Photoacoustic techniques

4.1 Experimental issues

The electrochemical cell (two electrodes configuration) was coupled with an open photoacoustic cell [24]. In this kind of configuration, the incident radiation comes from the front, and the sensor (*e.g.*, piezoelectric transducer [22, 23] or electret microphone [24, 25]) is located at the back of the Si substrate. A p-type Si is usually used because the *I-V* curve does not change as a function of the lighting conditions. These experiments were carried out using heavy doped silicon (p^+), single polished and $\langle 100\rangle$-oriented. The electrolyte composition is a HF/ethanol solution. A controlled current source (6220 Precision Current Source Brand Keithley) was used to fix a constant current profile and solid Cu back contact. As an excitation source, it requires a Si super-bandgap laser ($\lambda > 1107$ nm).

Figure 5 shows the PA amplitude recorded during the etching of Si. Initially, the electrochemical cell is empty. A few seconds later, the electrolyte is emptied. As a result, a perturbation of DC level takes place. It waits for another time interval for SiO_2 removal, and finally, the current source is turned on, producing an oscillatory shape in the PA amplitude. The PSi amplitude is a periodic function as a function of time. In the case of the Figure 5 the sample was etching during 32 PA cycles.

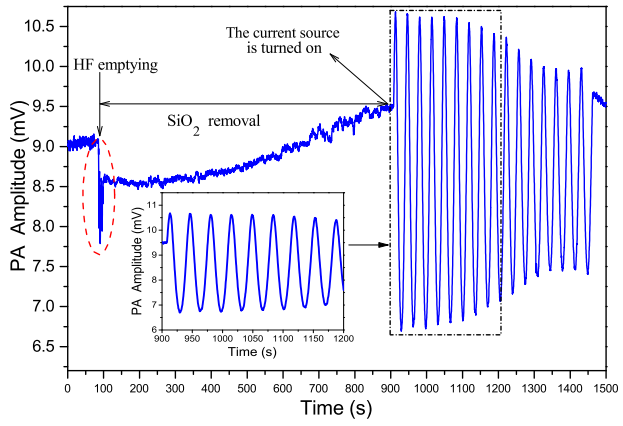

Figure 5: The experimental data of the PA amplitude signal as a function of time during 16 PA cycles. It was used a p^+-Si (0.005 Ω/cm) anodized at 20 mA/cm^2 and $\lambda_0 = 808$ nm.

4.2 Photoacoustic Modeling

The classical theory of photoacoustic proposes to solve the heat flow equations in this multilayered system to determine the temperature distribution. In the case of the formation of a PSi single layer, three interfaces appear as the Figure 2 shown. Electrolyte/PSi at $x = -(l_b + l)$, PSi/Si at $x = -l_b$, and Si/Air at $x = 0$. The coordinate origin is located conveniently at the end of the Si substrate, and the distance of the detection is at $x = l_g$, that it is the thickness of the gas column. The l is the thickness of the PSi, l_b the thickness of the Si backing. The general heat equation can be written as

$$\nabla^2 T_n(x,t) - \frac{1}{\alpha_n}\frac{\partial T_n(x,t)}{\partial t} = f_n(x,t) + Q_n(t,x), \qquad (14)$$

where, $f_n(x,t)$ are the optical heat sources, $Q_n(x,t)$ is a term related with the chemical reaction and Joule effect, and $n = 1, 2, 3$ refers to the heat diffusion medium (see Figure 2).

Experimentally, the periodical profile of the modulated light source is rectangular. However, if it is expanded in Fourier series and it takes the first harmonic; the function can be written as

$$f_n(x,t) = \frac{\beta_n I_n \eta_n \left(1 - R(t)\,|_{x=x_0}\right)}{2k_n} e^{\beta_n x}\left(1 + e^{i\omega t}\right), \qquad (15)$$

where β_n is the absorption coefficient, I_n is the intensity of the incident light, η_n is the quantum absorption efficiency, ω is the modulated frequency, k_n the thermal conductivity, and $R(t)$ is the reflectance evaluated at $x = x_0$. At this point, because the PSi/Si interface is moving as $l_b(t) = l_b(0) - vt$; where v is the formation velocity of PSi, the value of the reflectance is not constant. Thus, it is necessary to introduce the changes in the reflectance as follows.

$$R(t) = \left|r^2\right| = \frac{\cos^2(\delta)(\xi_0 - \xi_1)^2 + \sin^2(\delta)(\xi_0\xi_1 - 1)^2}{\cos^2(\delta)(\xi_0 + \xi_1)^2 + \sin^2(\delta)(\xi_0\xi_1 + 1)^2}, \qquad (16)$$

$$\delta(t) = \frac{2\pi n_2(p) l(t)}{\lambda_0}, \qquad (17)$$

where $\xi_0 = n_1/n_2(p)$, $\xi_1 = n_3/n_2(p)$, n_i the refractive index of each medium, which in the case of PSi ($n_2(p)$) is porosity (p) dependent. The inspection of the Equations 16 and 17 shows that the reflectance depends on the effective refractive index [48], the thickness of the PSi film, and the wavelength (λ_0) of the light source. Furthermore, the reflectance is a periodic function producing a self-modulation effect in the intensity of the incident light. This is the effect that produces the periodicity in the photoacoustic (PA) signal (see Figure 5). Admittedly, it is not convenient to introduce the expression of the Equation 16 in the heat equation. Even so, if it uses an approximation in Fourier series, the heat sources for each region can be written as,

for PSi region, $-(l + l_b) < x < -l_b + vt$

$$f_2(x,t) = -A(1 + e^{i\omega_1 t})e^{-\beta_2(x + l_b + l)} - B(1 + e^{i\omega_2 t})e^{\beta_2(x + l_b + vt)}, \qquad (18)$$

where

$$A = \frac{\beta_2 I_{1t}\eta_3}{2k_2} \text{ and } B = \frac{\beta_2 I_{1r}\eta_2}{2k_2}. \qquad (19)$$

For Si substrate, $-l_b + vt < x < 0$

$$f_3(x,t) = -C(1 + e^{i\omega_1 t})e^{-\beta_3(x + l_b + vt)} - D(1 + e^{i\omega_2 t})e^{\beta_3 x}, \qquad (20)$$

where

$$C = \frac{\beta_3 I_{1t}\eta_3}{2k_3} \text{ and } D = \frac{\beta_3 I_{1r}\eta_3}{2k_3}. \qquad (21)$$

For the gas, $0 < x < l_g$

$$f_4(x,t) = 0. \qquad (22)$$

By using the methodology developed for Rosencwaig and Gersho (RG) [25, 52] the temperature distribution in the cell is

$$T(x,t) = \mathrm{Re}\left\{\phi(x,t)\right\} + T_0, \qquad (23)$$

where T_0 is the room temperature and $\phi(x,t) = \phi_i(x,t)$ is given for each region as

$$\phi_2(x,t) = \phi_2^{\mathrm{DC}}(x,t) - \alpha_2 \int_0^t Q(\tau)d\tau \qquad (24)$$

$$+\left[W_1 e^{-\sigma_2^1(0)(x+l+l_b)} + W_2 e^{\sigma_2^1(0)(x+l+l_b)} - E_1 e^{-\beta_2(x+l+l_b)}\right] e^{i\omega_1 t} + \left[W_3 e^{-\sigma_2^2(v)(x+l_b+vt)} + W_4 e^{\sigma_2^2(v)(x+l_b+vt)} - E_2 e^{\beta_2(x+l_b+vt)}\right] e^{i\omega_2 t},$$

$$\phi_3(x,t) = \tilde{\phi}_3(x,t) + \left[U_1 e^{-\sigma_3^1(v)(x+l_b+vt)} - V_1 e^{-\beta_3(x+l_b+vt)}\right] e^{i\omega_1 t} + \left[U_2 e^{\sigma_3^2(0)x} - V_2 e^{\beta_3 x}\right] e^{i\omega_2 t}, \tag{25}$$

$$\phi_4(x,t) = \tilde{\phi}_4(x,t) + \sum_{n=1}^{2} \theta_n \exp\left[-\sigma_4^n x + i\omega_n t\right]. \tag{26}$$

The parameter σ_i is related with thermal diffusivity of every single media as

$$\sigma_j^n(v) = \frac{1}{2}\left(\frac{v}{2} + \frac{\sqrt{v^2 + 4i\alpha_j\omega_n}}{\alpha_j}\right), \quad j = 2, 3. \tag{27}$$
$$\sigma_4^n = (1+i)\sqrt{\frac{\omega_n}{2\alpha_g}},$$

and the coefficients E_j, U_j, V_j, and W_j are obtained by substitution of these expressions [25] (equations 24, 25, and 26) in the equation 14 with the following boundary conditions:

$$\begin{aligned} \phi_2(-l_b + vt, t) &= \phi_3(-l_b + vt, t) \\ \phi_3(0,t) &= \phi_4(0,t) \\ k_3\frac{\partial\phi_3}{\partial x}(-l_b + vt, t) &= k_2\frac{\partial\phi_2}{\partial x}(-l_b + vt, t), \\ k_4\frac{\partial\phi_4}{\partial x}(0,t) &= k_3\frac{\partial\phi_3}{\partial x}(0,t). \end{aligned} \tag{28}$$

Furthermore, the conditions mentioned above can be applied separately to each region to obtain the amplitude of the temperature evaluated at the length of the Si substrate, ($x = 0$) giving as a result:

$$\theta_1 = \frac{k_3(\beta_3 - \sigma_3^1(v))}{k_3\sigma_3^1(v) - k_4\sigma_4^1} V_1 e^{-\beta_3(l_b - vt)}, \tag{29}$$
$$\theta_2 = \frac{k_3(\beta_3 - \sigma_3^2(0))}{k_3\sigma_3^2(0) + k_4\sigma_4^2} V_2.$$

The temperature field is a function of time and space. However, the microphone just detects the pressure variations as a function of time, thus it is convenient to define the average temperature as follows

$$\bar{\phi}(t) \equiv \frac{1}{2\pi\mu_4}\int_0^{2\pi\mu_4} \phi_{AC}(x,t)dx. \tag{30}$$

When this average definition is applied to the equation 26,

$$\bar{\phi}(t) \approx \sum_{n=1}^{2}\sqrt{\frac{\alpha_4}{\omega_n}}\theta_n e^{i(\omega_n t - \pi/4)}. \tag{31}$$

is obtained, where μ_4 is the thermal diffusion length of the gas ($\mu_i = \sqrt{2\alpha_i/\omega}$). Finally, by using the gas ideal approximation, the displacement of the column gas is

$$\delta x(t) = 2\pi\mu_4 \sum_{n=1}^{2}\sqrt{\frac{\alpha_4}{\omega_n}}\frac{\theta_n}{\Phi} e^{i(\omega_n t - \pi/4)}, \tag{32}$$

where the average DC temperature of the gas is set equal to the DC solid surface, thus $\Phi = \theta_0 + T_0$, and the adiabatic pressure variations is

$$\delta P(t) = \gamma\frac{P_0}{V_0}\delta V(t) = \gamma P_0 \frac{2\pi\mu_4}{l_g}\sum_{n=1}^{2}\sqrt{\frac{\alpha_4}{\omega_n}}\frac{\theta_n}{\Phi} e^{i(\omega_n t - \pi/4)}. \tag{33}$$

4.3 Data fitting and results

Figure 6 shows a fitting example of the experimental data shown in the figure 5. For the fit procedure, the experimental values of thermal and optical parameters for Si were extracted from Ramirez-Gutierrez et al. [25]. In this case, the modulation frequency of the light was $f = 13$ Hz, and the sample was etched during 16 PA cycles. It is necessary to fit at least one PA cycle to find the etch rate or the formation velocity. The amplitude of the PA signal decreases as a function of the PSi thickness due to absorption, scattering, and coherence loss [53], and the DC level increases because of the Joule effect and the chemical reaction. Consequently, fluctuations during the etching take place producing changes in the PSi formation velocity. As a consequence, the PA signal is fitted by sections, and the frequency parameter (ω_2 in equations 18 and 20) related to the velocity was obtained.

In the case of Figure 6, a combination of velocities formation (v_i) and frequencies (ω_{2i}) is used to fit the PA cycles. Also, the absorption coefficient remains as a constant.

Figure 7 shows a ratio between the experimental data and the theoretical model. It shows the accuracy of the model is of about 90%. In this case, due to change in the formation velocity, the data was fit into sections that were defined arbitrarily. Each velocity is represented in a different color, and it is related to a change in the period of the PA cycle. In general, the model provides a good description of the phenomenology. A better fit of the experimental data can be achieved by considering several velocities

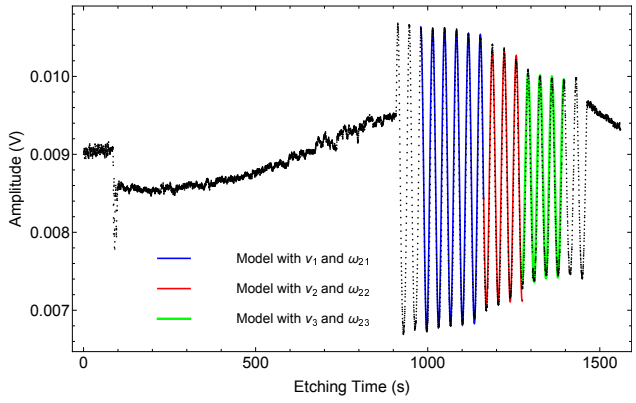

Figure 6: The experimental data (black line) and the fitting (color line blue, red and green) Each section was fit by using a different frequency, it means that the formation velocity does not remain constant along the chemical reaction.

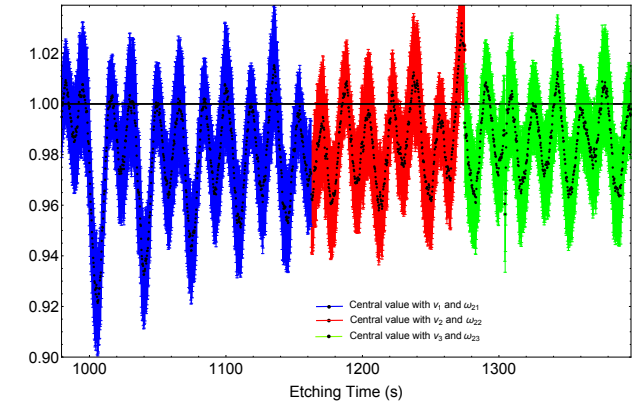

Figure 7: The ratio between the data and theory. Black dots represent the central value of the ratio. (Color line) Represent the error bars associated with the uncertainty related to the experimental performance.

in short intervals of time, in fact,a short-time Fourier transformed is recommended to extract all the frequency components. Also, it is recommended to control the noise during the data acquisition.

Figure 8 shows the velocity formation of the porous layer as a function of the etching time. In this case, two samples were grown under different conditions. In the case of the sample previously reported by by Ramirez-Gutierrez et al. [25], the velocity formation of the PSi remains constant during 500 s. However, a sharp jump takes place at 1150 s that it is an indicative of perturbation on growth conditions. In the case of long time etching, it is reported that the composition of the electrolyte changes and the increase in the temperature modifies the chemical reaction.

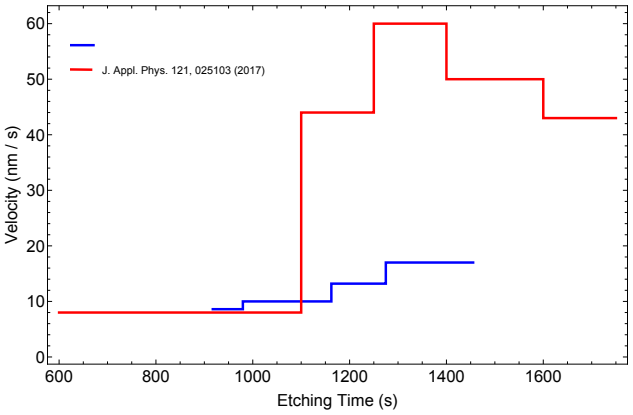

Figure 8: ((Blue line) Formation velocity as a function of the time for the sample shown in figure 5. (Red line) It shows the case studied in the reference [25]. This graphic shows that the formation velocity of PSi is not constant along the reaction.

5 Conclusions

Porous silicon (PSi) has been considered as a versatile material for optoelectronics, chemical sensing, an anode for lithium batteries, among others applications in several fields. These new forms of surface modified silicon or porous silicon (PSi) involve the design and construction of single or multi- thin films structures. Of course, the growth of PSi or the process to make porous requires the implementation of real time (in-situ) techniques that can provide control and accuracy in the physicochemical properties. Techniques such as optical interferometry and photoacoustics can be enhance the reproducibility of standard methods to obtain PSi. This fact represents an advantage over the ex-situ techniques to characterize the properties of PSi. The in-situ monitoring and characterization of the PSi formation opens a new window for a better understanding of the route for the porous nucleation in Si and liquid/semiconductor interface. Also, it propels the applications of PSi because it allows control of its properties. Also, it generates an optimization in the growth and fabrication process.

In the case of interferometry, the methods presented show a methodology real-time monitoring of multiple parameters of PSi, such as the velocity formation, porosity profile, refractive index, and roughness. It allows studying the effect of the electrolyte composition and temperature to characterize the evolution of surface morphology. Nevertheless, multiple reflections in the interfaces produce more than one frequency component in the reflected amplitude. In this case, it is necessary to take into account all possible reflections and extract all the frequency parameters by Fourier analysis.

In the case of photoacoustics, the primary mechanism to generate the signal (sound) is the absorption of modulated light, despite the fact that PA signal is governed by interference effects, a diffusive process creates the PA signal that produces a decrease of frequency components in the signal which is an advantageous situation for monitoring multilayer systems such as Bragg reflector. A simple analysis of the maxima and minima points of the PA signal can provide criteria to calculate the effective refractive index of the PSi film that is the case reported by Ramirez-Gutierrez et al. [24]. Moreover, if the heat equation for the multilayer system is solved, it is possible to reproduce the PA signal by using fitting parameters such as the oscillation frequency and velocity formation. The PSi signal also contains information about the increase of temperature during the etching process, that is an indication that the PA signal includes information on the chemical reaction and thermal properties of the system that makes an attractive scenario to study thermal properties of porous media. In addition, the photoacoustic method can be used for monitoring the formation of a multilayered system making photoacoustic a useful technique for the fabrication of photonic crystal based on PSi. Finally, these methods are no surface-specific but are useful to characterize macroscopic properties, such as the formation velocity, film thickness, roughness, refractive index, and thermal conductivity.

Acknowledgement: C. F. Ramirez-Gutierrez and J. D. Castaño-Yepes want to thank Consejo Nacional de Ciencia y Tecnología México (CONACYT), for the financial support of their Ph.D. studies. Authors thank Beatriz Millan-Malo Ph.D., for the simulations support. We acknowledge the English editing by Kevin Maya-Martinez from Universidad del Quindio.

References

[1] Liz-Marzán, L. M. & Giersing, M. (Eds.), Low-Dimensional Systems: Theory, Preparation, and Some Applications. Kluwer Academic Publishers, Dordrecht, 2003.

[2] Tao, F. F. & Bernasek, S. L., Functionalization of Semiconductor Surfaces. John Wiley & Sons, New Jersey, 2012.

[3] Vaseashta, A. & Mihailescu, I. N., Functionalized Nanoscale Materials, Devices and Systems. Springer Science + Business Media B.V., Dordrecht, 2008.

[4] Hayner, C. M., Zhao, X., & Kung, H. H., Materials for rechargeable lithium-ion batteries. Annu. Rev. Chem. Biomol. Eng. 3, 2012, 445-471.

[5] Lee, J. K., Smith, K. B., Hayner, C. M., & Kung, H. H., Silicon nanoparticles–graphene paper composites for Li ion battery anodes. Chem. Commun. 46, 2010, 2025–2027.

[6] Cheng, Y. W., Lin, C. K., Chu, Y. C., Abouimrane, A., Chen, Z., Ren, Y., et al., Electrically Conductive Ultrananocrystalline Diamond-Coated Natural Graphite-Copper Anode for New Long Life Lithium-Ion Battery. Adv. Mater. 26(22), 2014, 3724–3729.

[7] Ge, M., Fang, X., Rong, J., & Zhou, C., Review of porous silicon preparation and its application for lithium-ion battery anodes. Nanotechnology 24, 2013, 422001.

[8] Canham, L., Handbook of Porous Silicon, Springer International Publishing, Switzerland, 2014.

[9] Smoth, R. L. & Collins, S. D., Porous silicon formation mechanisms. J. Appl. Phys. 71(8), 1992, R1–R22.

[10] Rao, A. V., Ozanam, F., Chazalviel, J. N., In Situ Fourier-Transform Electromodulated Infrared Study of Porous Silicon Formation: Evidence for Solvent Effects on the Vibrational Linewidths. J. Electrochem. Soc. 138, 1991, 153–159.

[11] Dietrich, R., Grobe, J., & Feldb, H., In-situ FT-IR Studies of Porous Silicon Surface Reactions. J. Mol. Struct. 349, 1995, 109-112.

[12] Thönissen, M., Berger, M. G., Billat, S., Arens-Fischer, R., Krüger, Lüth, M.,H., et al., Analysis of the depth homogeneity of p-ps by reflectance measurements. Thin Solid Films 297, 1997, 92–96.

[13] Steinsland, E., Finstad, T., & Hanneborg, A., Laser reflectance interferometry for In Situ determination of silicon etch rate in various solutions. J. Electrochem. Soc. 146 (10), 1999, 3890–3895.

[14] Pavesi, L., Gaburro, Z., Dal Negro, L., Bettotti, P., Vijaya Prakash, G., Cazzanelli, M.; et al., Nanostructured silicon as a photonic material. Opt. Lasers Eng. 39, 2003, 345–368.

[15] Gaburro, Z., Oton, C. J., Bettotti, P., Dal Negro, L., Vijaya Prakash, G., Cazzanelli, M.; et al., Interferometric Method for Monitoring Electrochemical Etching of Thin Films. J. Electrochem. Soc. 150 (6), 2003, C381-C384.

[16] Foss, S. E., Kan, P. Y. Y., & Finstad, T. G., Single beam determination of porosity and etch rate in situ during etching of porous silicon, J. Appl. Phys. 97, 2005, 114909–114911.

[17] Kan, P. Y. Y., Foss, S. E., & Finstad, T. G., The effect of etching with glycerol, and the interferometric measurements on the interface roughness of porous silicon. Phys. Stat. Sol. (a) 202 (8), 2005, 1533–1538.

[18] Dietz, N., Real-time optical characterization of thin films growth. Mater. Sci. Eng. B 87, 2001, 1–22.

[19] Zhao, Y. P., Yang, H. N., Wang, G. C., & Lu, T. M., Extraction of real-space correlation function of a rough surface by light scattering using diode array detectors. Appl. Phys. Lett. 68, 1996, 3063-3065.

[20] Zhao, Y. P., Yang, Y. J. W. N., Wang, G. C.', & Lu, T. M., In situ real-time study of chemical etching process of Si(100) using light scattering. Appl. Phys. Lett. 69, 1996, 221–223.

[21] Espinosa-Arbeláez, D. G., Velázquez-Hernández, R., Petricioli-Carranco, J., Quintero-Torres, R., & Rodríguez-García, M. E., Differential photoacoustic cell to study the wetting process during porous silicon formation. Phys. Status Solidi C 8(6), 2011, 1856–1859.

[22] Andrusenko, D., Isaiev, M., Kuzmich, A., Lysenko, V., & Burbelo, R., Photoacoustic effects in nanocomposite structure porous silicon-liquid. Nanoscale Res. Lett. 7, 2012, 411.

[23] Isaiev, M., Voitenko, K., Doroshchuka, V., Andrusenkoa, D., Kuzmicha, A., Skryshevskiia, A., et al., Thermal Elasticity Stresses Study in Composite System Porous Silicon-Liquid. Phys. Procedia 70, 2015, 586–589.

[24] Ramirez-Gutierrez, C. F., Castaño-Yepes, J. D., & Rodriguez-García, M. E., In situ photoacoustic characterization for porous silicon growing: Detection principles. J. Appl. Phys. 119, 2016, 185103-1 – 185103-7.

[25] Ramirez-Gutierrez, C. F., Castaño-Yepes, J. D., & Rodriguez-García, M. E., Modeling the photoacoustic signal during the porous silicon formation. J. Appl. Phys. 121, 2017, 025103.

[26] Mandal, K. C., Ozanam, F., & Chazalviel, J. N., In situ infrared evidence for the electrochemical incorporation of hydrogen into Si and Ge. Appl. Phys. Let. 57, 1990, 2788–2790.

[27] Koch, F., Petrova-Koch, V., & Muschik, T., The luminescence of porous Si: the case for the surface state. J. Lumin. 57, 1993, 271–281.

[28] Dubin, V. M., Ozanam, F., & Chazalviel, J. N., In situ infrared spectroscopic study of luminescent porous silicon. Vib. Spectrosc. 8, 1994, 159–166.

[29] Saar, A., Photoluminescence from silicon nanostructures: The mutual role of quantum confinement and surface chemistry. J. Nanophoton. 3(1), 2009, 032501.

[30] Ramirez-Gutierrez, C. F., Medina-Herrera, A., Tirado-Mejía, L., Zubieta-Otero, L. F., Auciello, O., & Rodriguez-Garcia, M. E., Photoluminescence study of porous p-type silicon: Identification of radiative transitions. J. Lumin. 201, 2018, 11–17.

[31] John, G. C. & Singh, V. A., Self-organization in porous silicon formation. Phys. Rev. B 56(8), 1997, 4638–4641.

[32] Hess, P., Photoacoustic, Photothermal and Photochemical Processes at Surfaces and in Thin Films, Springer-Verlag, Berlin, 1989.

[33] Amato, G., Benedetto, G., Boarino, L., Brunetto, N., & Spagnolo, R., Photothermal and photoacoustic characterization of porous silicon. Opt. Eng. 36(2), 1997, 423–431.

[34] Toyoda, T., Takahashi, T., & Shen, Q., Photoacoustic and photoluminescence studies of porous silicon etched by low-concentration hydrofluoric acid. J. Appl. Phys. 88, 2000, 6444–6450.

[35] Kawahara, T., Morimoto, J., Tahira, K., & Miyakawa, T., Effects of boundary reflection on photoacoustic spectrum of porous silicon. Appl. Phys. A 70(4), 2000, 407-–409.

[36] Lehmann, V. & Gösele, U., Porous silicon formation: A quantum wire effect. Appl. Phys. Lett. 58, 1991, 856–858.

[37] Zhang, X. G., Morphology and formation mechanisms of porous silicon. J. Electrochem. Soc. 151, 2004, C69–C80.

[38] Itano, M., Kern, F. W., Miyashita, M., & Ohmi, T., Particle removal from silicon wafer surface in wet cleaning process. IEEE Trans. Semicond. Manuf. 6(3), 1993, 258–267.

[39] Kern, W., The Evolution of Silicon Wafer Cleaning Technology. J. Electrochem. Soc. 137(6), 1990, 1887–1892.

[40] A. Podolian,A. Nadtochiy, V. Kuryliuk, O. Korotchenkov, J. Schmid, M. Drapalik; et al, The potential of sonicated water in the cleaning processes of silicon wafers, Sol. Energy Mater Sol. Cells 95 (2), 765-772 (2011)

[41] Setzu, S., Lérondel, G., & Romestain, R., Temperature effect on the roughness of the formation interface of p-type porous silicon. J. Appl. Phys. 84(6), 1998, 3129–3133.

[42] G. Koster & Rijnders, G., In situ characterization of thin film growth, Woodhead Publishing Limited, Cambridge, 2011.

[43] Fried, M. & Rédei, L., Non-destructive optical depth profiling and real-time evaluation of spectroscopic data. Thin Solid Films 364, 2000, 64–74.

[44] Baklanov, M. R., Mogilnikov, K. P., Polovinkin, V. G., & Dultsev, F. N., Determination of pore size distribution in thin films by ellipsometric porosimetry. J. Vac. Sci. Technol. B 18, 2000, 1385–1391.

[45] Kaminska, K., Amassian, A., Martinu, L., & Robbie, K., Growth of vacuum evaporated ultraporous silicon studied with spectroscopic ellipsometry and scanning electron microscopy. J. Appl. Phys. 97, 2005, 013511.

[46] Prabakaran, R., Raghavan, G., Sundari, S. T., Kesavamoorthy, R., & Xavier, F. P., Ellipsometry studies on the effect of etching time in porous silicon. Physica E Low Dimens Syst Nanostruct 15(4), 2002, 243–251.

[47] Schmid, P. E., Optical absorption in heavily doped silicon. Phys. Rev. B 23(10), 1981, 5531–5536.

[48] Choy, T. C., Effective Medium Theory Principles and Applications, 2nd ed., Oxford University Press, Oxford, 2016.

[49] Alius, H. & Schmidt, R., Interference method for monitoring the refractive index and the thickness of transparent films during deposition. Rev. Sci. Instrum. 61, 1990, 1200–1203.

[50] Lérondel, G. & Romestain, R., Fresnel coefficients of a rough interface. Appl. Phys. Lett. 74, 1999, 2740.

[51] Lérondel, G., Romestain, R., & Barret, S., Roughness of the porous silicon dissolution interface. J. Appl. Phys. 81, 1997, 6171–6178.

[52] Ronsencwaig, A. & Gersho, A., Theory of the photoacoustic effect with solids. J. Appl. Phys. 47(64), 1976, 64–69.

[53] Mitsas, C. L. & Siapkas, D. I., Generalized matrix method for analysis of coherent and incoherent reflectance and transmittance of multilayer structures with rough surfaces, interfaces, and finite substrates. Appl. Opt. 34(10), 1995, 1678–1683.